This is an open access article published under an ACS AuthorChoice License, which permits copying and redistribution of the article or any adaptations for non-commercial purposes.

ACS AuthorChoice

ACS NANO

www.acsnano.org

ARTICLE

Threading through Macrocycles Enhances the Performance of Carbon Nanotubes as Polymer Fillers

Alejandro López-Moreno,[†] Belén Nieto-Ortega,[†] Maria Moffa,[‡] Alberto de Juan,[†] M. Mar Bernal,[†] Juan P. Fernández-Blázquez,[§] Juan J. Vilatela,[§] Dario Pisignano,[*,‡,∥] and Emilio M. Pérez[*,†]

[†]IMDEA Nanoscience, Ciudad Universitaria de Cantoblanco, C/Faraday 9, 28049 Madrid, Spain

[‡]Istituto Nanoscienze-CNR, Euromediterranean Center of Nanomaterial Modelling and Technology (ECMT), via Arnesano, 73100 Lecce, Italy

[§]IMDEA Materials, Eric Kandel 2, Getafe, 28005 Madrid, Spain

[∥]Dipartimento di Matematica e Fisica "Ennio De Giorgi", Università del Salento, via Arnesano, 73100 Lecce, Italy

Supporting Information

ABSTRACT: **In this work, we study the reinforcement of polymers by mechanically interlocked derivatives of single-walled carbon nanotubes (SWNTs). We compare the mechanical properties of fibers made of polymers and of composites with pristine SWNTs, mechanically interlocked derivatives of SWNTs (MINTs), and the corresponding supramolecular models. Improvements of both Young's modulus and tensile strength of up to 200% were observed for the polystyrene−MINT samples with an optimized loading of just 0.01 wt %, while the supramolecular models with identical chemical composition and loading showed negligible or even detrimental influence. This behavior is found for three different types of SWNTs and two types of macrocycles. Molecular dynamics simulations show that the polymer adopts an elongated conformation parallel to the SWNT when interacting with MINT fillers, irrespective of the macrocycle chemical nature, whereas a more globular structure is taken upon facing with either pristine SWNTs or supramolecular models. The MINT composite architecture thus leads to a more efficient exploitation of the axial properties of the SWNTs and of the polymer chain at the interface, in agreement with experimental results. Our findings demonstrate that the mechanical bond imparts distinctive advantageous properties to SWNT derivatives as polymer fillers.**

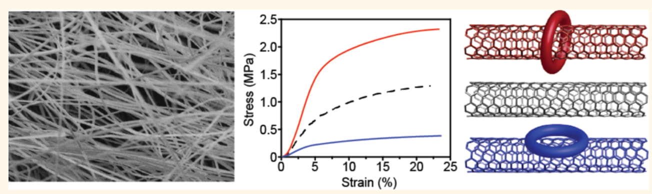

KEYWORDS: *electrospinning, nanotubes, mechanical properties, polymers, rotaxanes*

Carbon nanotubes are extensively used as reinforcing fillers in composites due to their extraordinary mechanical and structural properties. Since the report in this field by Ajayan *et al.*,[1] several materials where the mechanical and/or electrical properties of polymers have been significantly improved through nanotubes fillers have been demonstrated and used for different applications,[2−16] including improved batteries, mechanically reinforced materials,[17,18] and sensors.[19,20]

To fully exploit the properties of single-wall carbon nanotubes (SWNTs) as fillers in polymer matrices, a lot of research has been directed toward their chemical modification. In this framework, the mechanical bond is very attractive due to its dynamic features,[21,22] which have allowed for the construction of artificial molecular machines.[23−30] The mechanical bond is also very relevant for polymer science: polyrotaxanes, polycatenanes, and supramolecular polymers including mechanically interlocked molecules have all been investigated.[31−39] The reinforcement effect of B/SiOx nanocomposites through the formation of interlocked "necklaces" has also been described.[40,41]

The mechanical link was recently introduced by some of us as a tool for the chemical manipulation of SWNTs.[42−45] We used a U-shaped precursor featuring two units of a recognition element for SWNTs connected through an aromatic spacer and further decorated with alkene-terminated alkyl spacers of different lengths. Using pyrene and π-extended derivatives of tetrathiafulvalene, both of which have high affinity for SWNTs,[46−49] we could template the ring-closing metathesis (RCM) of the U-shaped precursor around the nanotubes, forming mechanically interlocked derivatives of SWNTs (MINTs, Figure 1a). Thanks to the extreme aspect ratio of the nanotubes, which prevents dissociation of the macrocycles from the nanotubes once they are

Received: June 17, 2016
Accepted: July 25, 2016
Published: July 25, 2016

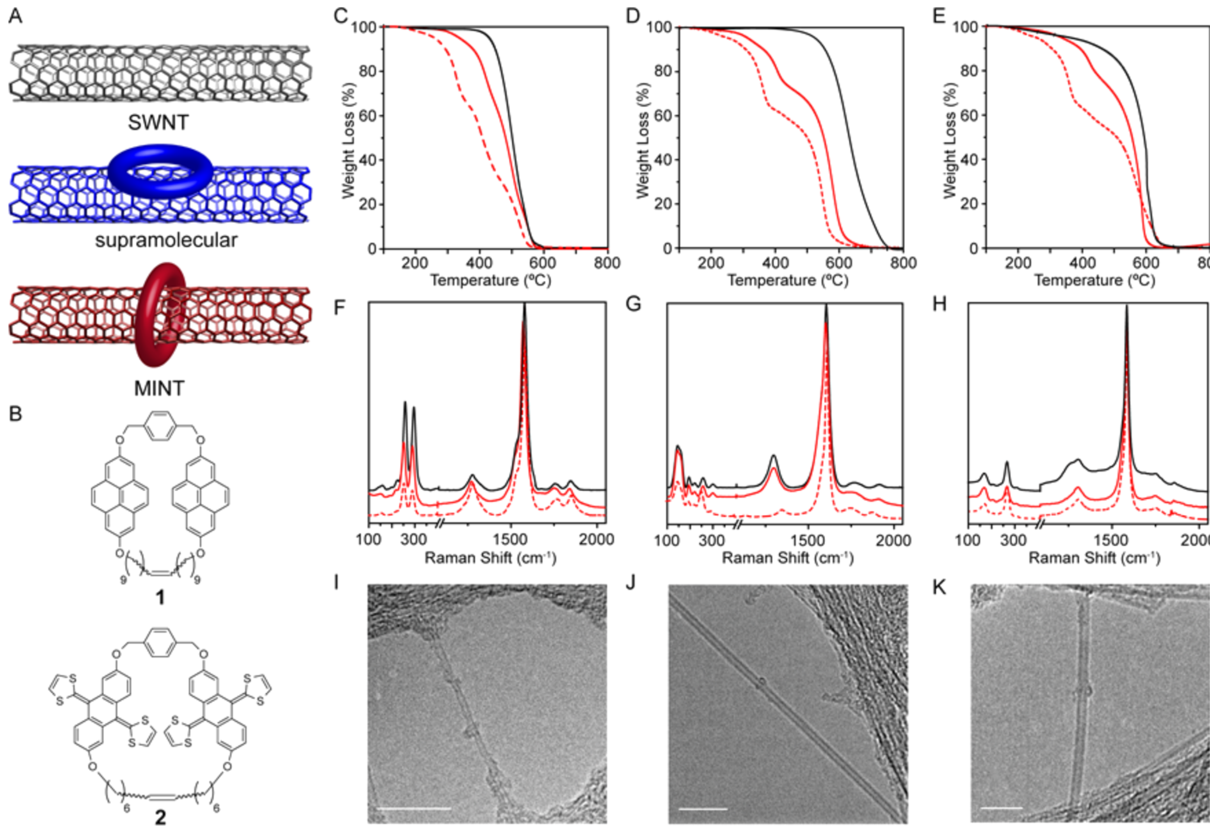

Figure 1. (a) Schematic representation of the three fillers investigated: SWNTs, supramolecular associates, and MINTs. (b) Chemical structure of macrocycles 1 and 2. (c−k) Characterization of MINT derivatives. TGA analysis of (c) pristine (6,5)-SWNTs (black), $MINT_{(6,5)}$−1 (red), and $MINT_{(6,5)}$−2 (dashed red); (d) pristine pp-SWNTs (black), $MINT_{(pp)}$−1 (red), and $MINT_{(pp)}$−2 (dashed red); (e) pristine o-SWNTs (black), $MINT_{(o)}$−1 (red), and $MINT_{(o)}$−2 (dashed red); Raman spectra of (f) (6,5)-SWNTs (black), $MINT_{(6,5)}$−1 (red), and $MINT_{(6,5)}$−2 (dashed red); (g) pp-SWNTs (black), $MINT_{(pp)}$−1 (red), and $MINT_{(pp)}$−2 (dashed red); (h) o-SWNTs (black), $MINT_{(o)}$−1 (red), and $MINT_{(o)}$−2 (dashed red); TEM images of nanotubes (showing macrocycles around nanotubes) in (i) $MINT_{(6,5)}$−2; (j) MINT $_{(pp)}$−2, and (k) $MINT_{(o)}$−2. Scale bars are 10 nm. TGAs were run in air at a heating rate of 10 °C min^{-1}. All Raman spectra are the average of 10 different measurements at λ_{exc} = 785 nm.

formed around them, MINTs showed stability comparable to that of covalently modified nanotubes while maintaining the native structure of the SWNTs. Since rotaxanes and pseudorotaxanes are both topologically identical,[50,51] and the major difference between them is their kinetic stability,[52] we believe our MINT derivatives can be considered mechanically interlocked despite the lack of explicit stoppers.

To effectively transfer the anisotropic properties of elongated fillers such as SWNTs to composites, a parallel orientation in the matrix and a strong interaction with the polymer are required. In principle, the parallel orientation along the prevalent direction of macromolecular chains can be favored by electrospinning, due to the very high elongational strain rates applied,[53−55] while the noncovalent interactions between polymer and filler can be tuned chemically. Recently, the groups led by Pisignano and Credi have described that various dynamic properties of rotaxane-type molecules are conserved within electrospun fibers.[56]

Here, we present our results on the influence of the mechanical bond on the mechanical properties of SWNT-based nanocomposites. We incorporate MINTs in polystyrene fibers and study their tensile properties. The merits of the MINT functionalization approach manifest as substantial enhancements in Young's modulus and tensile strength. In comparison, noninterlocked model samples of identical chemical composition show no positive effect.

RESULTS AND DISCUSSION

We utilized two types of macrocycles (Figure 1b) and three types of SWNTs of different diameters, lengths, and electronic character. In particular, we used pyrene- (**1**) and exTTF-based (**2**) macrocycles and (6,5)-enriched nanotubes (0.7−0.9 nm in diameter, length ≥700 nm, mostly semiconducting, 95% purity) denoted as (6,5)-SWNTs, plasma-purified SWNTs (pp-SWNTs 0.8−1.6 nm in diameter, length 3−30 μm, mostly metallic, 99% purity), and shorter COOH functionalized SWNTs (o-SWNTs 0.8−1.6 nm in diameter, length 0.5−2.0 μm, mostly metallic, 99% purity). These various types of samples allowed us to discriminate mechanical reinforcement arising from differences in SWNT length or dispersion quality from those directly due to the MINT functionalization.

The general method for the synthesis of MINTs has been reported elsewhere.[42−45] Briefly, we use a clipping strategy in which a suspension of SWNTs is treated with the adequate bis-alkene U-shape precursor and Grubbs' second-generation catalyst. After supramolecular association of the U-shape, it can be closed around the SWNT to form MINTs. Noninterlocked macrocycles and U-shapes, oligomers, catalyst, and all other byproducts are removed by extensive washes with dichloromethane. The interlocked macrocycles stay in place without the need for "stoppers" due to the extreme aspect ratio of the SWNTs. All samples used in this study were adequately characterized by standard methods, including thermogravimetric

DOI: 10.1021/acsnano.6b04028
ACS Nano 2016, 10, 8012−8018

analysis (TGA), Raman, UV−vis−NIR, and TEM. Figure 1 shows representative examples of TGA curves, Raman spectra, and TEM micrographs. TGA evidence indicated that, following MINT-forming reaction, the SWNTs showed organic functionalization between 27 and 43%, remaining stable even after reflux in tetrachloroethane for 30 min. No major shifts and no increase in the I_D/I_G ratio upon functionalization were found in the Raman spectra, confirming that the functionalization is noncovalent. HRTEM allows visualization of individual macrocycles around the SWNTs in the MINT samples (for comprehensive characterization, including control experiments, see the Supporting Information and refs 42−45).

We prepared suspensions of the SWNT derivatives through ultrasonication. To avoid the presence of aggregates that could affect the mechanical properties, the suspensions were centrifuged and then polystyrene was added. Electrospinning was carried out using a commercially available system, operating with an applied interelectrode bias of 14 kV and a flow rate of 1 mL h^{-1}. The filler loading was optimized to 0.01 wt % respect to polystyrene, since larger loadings lead to defective fibers (Supporting Information). With this loading, fibers showed seamless and uniform surfaces, without discernible beads or nanotube aggregates. Figure 2 displays typical scanning electron

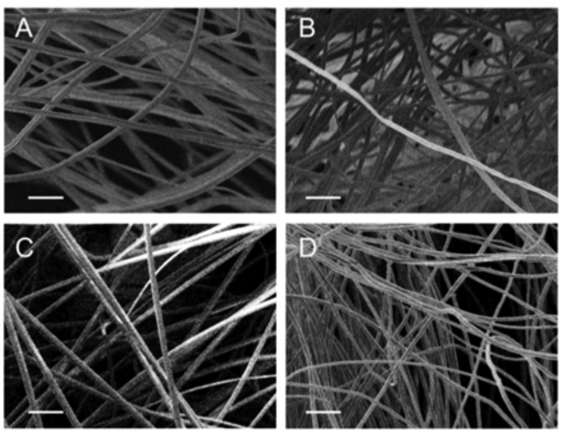

Figure 2. SEM images of (a) polystyrene fibers; (b) o-SWNTs; (c) MINT$_{(o)}$−1; (d) o-SWNTs·1. Inset scale: 10 μm.

(SEM) micrographs of fibers made of pristine polystyrene and of those with o-SWNT-based fillers as representative examples (other samples are shown in the Supporting Information).

The diameter distribution of the fibers is within the same range of 1.3−1.8 μm for all samples (Figure S7). Pristine polystyrene fibers are slightly thicker (2.2 ± 0.6 μm) as expected because of the lower solution conductivity.[57] The (6,5)-SWNTs and pp-SWNTs samples are similar to o-SWNTs in structure and size as shown in Figure S8. The mechanical properties of the fibers were then determined using a dynamic mechanical analyzer (DMA). Each nanocomposite (n = 3 specimens) was cut into 1 × 4 cm^2 pieces to define samples with thickness 0.15−0.18 mm. All samples had comparable area density (ca. 2.5 mg cm^{-2}), and thus, the test specimens had similar linear densities too, ensuring stable force to stress normalization in the measurements. Force−displacement curves were recorded at 1 N min^{-1} (up to 18 N).

Figure 3 displays stress/strain curves for reference polystyrene (gray) and the nanocomposites explored: with pristine SWNTs (black), SWNTs + macrocycle supramolecular complex (blue), and MINT (red) for all types of SWNTs. The MINT samples present substantially higher modulus, yield, and tensile strengths than all control samples. Interestingly, in the supramolecular systems, the macrocycle reduces dramatically both modulus and strength, suggesting that it acts as a plasticizer that weakens the SWNT/matrix interface. The traditional composite has similar tensile properties to the pure polystyrene matrix, including ductility. The implication is that at this low volume fraction even pure SWNTs are well dispersed, for otherwise in aggregated form they would most likely act as defects that would reduce ductility. This supports the view that the improvement in mechanical reinforcement obtained using the MINT strategy is due to a more efficient stress transfer across the SWNT/polymer interface (*vide infra*). The Young's moduli and tensile strengths of all samples are displayed in Figure 4 and Table S1.

General trends are clearly evidenced. First, the mechanical properties of fibers are only slightly reinforced by pristine SWNTs fillers. Second, the use of MINTs leads instead to a significant improvement of both the Young's modulus and the tensile strength in all samples, irrespective of the type of nanotube or macrocycle. Lastly, the supramolecular fillers have negligible or even detrimental effects on the mechanical properties of the polystyrene fibers. For instance, the samples in which pristine (6,5)-SWNTs were used as fillers showed a Young's modulus of 18 ± 1 MPa and a tensile strength of 1.26 ± 0.06 MPa, whereas the pure polystyrene fibers showed 15 ± 1 and 1.09 ± 0.03 MPa, respectively. In contrast, the MINT$_{(6,5)}$−**1** samples showed 32 ± 6 MPa and 2.0 ± 0.3 MPa, which is a remarkable improvement of 110% in the Young's modulus and of 80% in the tensile strength. Meanwhile, the supramolecular filler

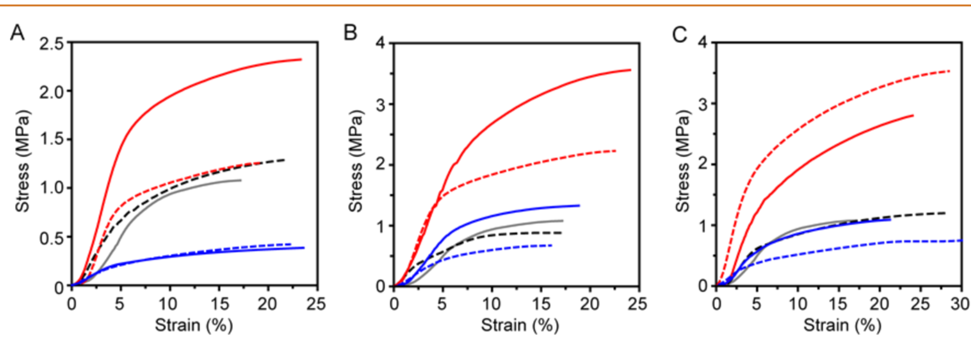

Figure 3. Representative stress/strain curves of (a) polystyrene (gray) and its composites with (6,5)-SWNTs (dashed black), MINT$_{(6,5)}$−1 (red), (6,5)-SWNTs·1 (blue), MINT$_{(6,5)}$−2 (dashed red), and (6,5)-SWNTs·2 (dashed blue); (b) polystyrene (gray) and its composites with pp-SWNTs (dashed black), MINT$_{(pp)}$−1 (red), pp-SWNTs·1 (blue), MINT$_{(pp)}$−2 (dashed red), and pp-SWNTs·2 (dashed blue); (c) polystyrene (gray) and its composites with o-SWNTs (dashed black), MINT$_{(o)}$−1 (red), o-SWNTs·1 (blue), MINT$_{(o)}$−2 (dashed red), and o-SWNTs·2 (dashed blue).

DOI: 10.1021/acsnano.6b04028
ACS Nano 2016, 10, 8012−8018

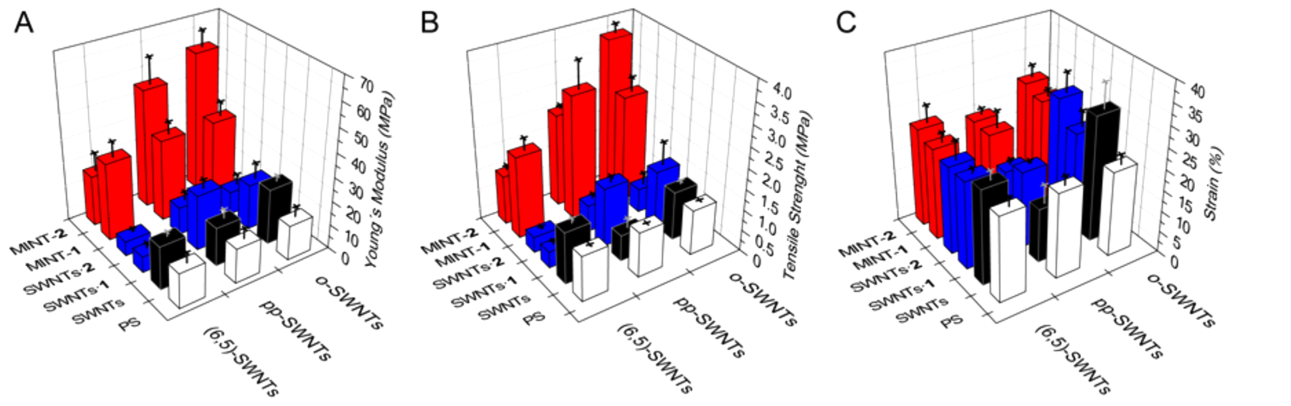

Figure 4. (a) Young's modulus of polystyrene (white), SWNTs (black), supramolecular complexes (blue), and MINTs (red) with (6,5)-SWNTs (left), pp-SWNTs (center), and o-SWNTs (right). (b) Tensile strength of polystyrene (white), SWNTs (black), supramolecular complexes (blue), and MINTs (red) with (6,5)-SWNTs (left), pp-SWNTs (center), and o-SWNTs (right). (c) Strain of polystyrene (white), SWNTs (black), supramolecular complexes (blue), and MINTs (red) with (6,5)-SWNTs (left), pp-SWNTs (center), and o-SWNTs (right).

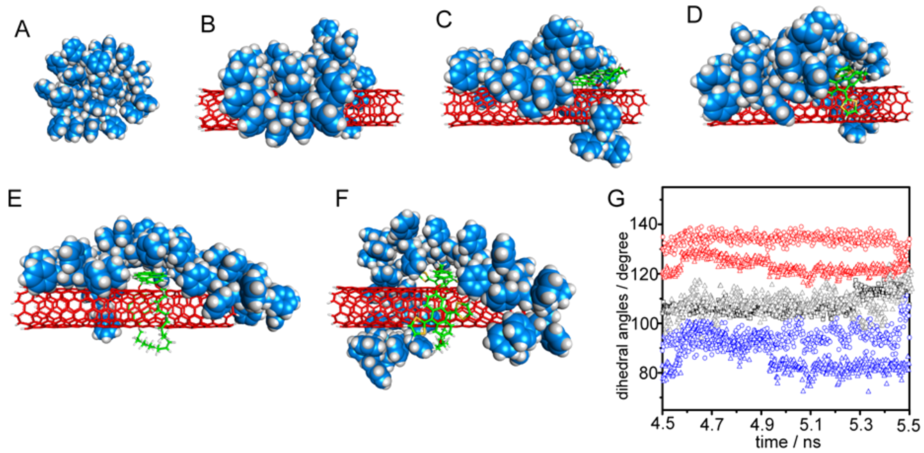

Figure 5. MD snapshots of (a) polystyrene and its composites with (b) SWNTs, (c) SWNT·**1**, (d) SWNT·**2**, (e) MINT−**1**, and (f) MINT−**2** after MD simulations. Carbon atoms are shown in red for the SWNTs, green for the macrocycles, and cyan for polystyrene. Hydrogens are shown in white, oxygen in red, and sulfur in yellow. (g) Average dihedral angles of the polystyrene backbone for the last nanosecond of the MD simulation. Color code: polystyrene (gray triangle) and its composites with SWNTs (black square), SWNT·**1** (blue circle), SWNT·**2** (blue triangle), MINT−**1** (red circle), and MINT−**2** (red triangle).

(6,5)-SWNTs·**1** yielded 7 ± 1 MPa and 0.39 ± 0.03 MPa as Young's modulus and tensile strength, respectively, which implies a variation of −53% in the Young's modulus and of −64% in the tensile strength with respect to the pristine polymer.

The trends for macrocycle **2** are identical, although with quantitatively smaller effects. In the case of pristine pp-SWNTs, we observed no significant variation in the Young's modulus and a decrease of −50% in the tensile strength with respect to polystyrene. Meanwhile, the $\mathrm{MINT}_{(pp)}$−**1** and $\mathrm{MINT}_{(pp)}$−**2** fillers showed an increase of 130% and 230% in the Young's modulus and 170% and 106% in the tensile strength, respectively. The supramolecular models showed very small improvements in the case of macrocycle **1** and slightly detrimental effects for macrocycle **2**.

Finally, for the pristine o-SWNT-filled samples, the variation in Young's modulus with respect to polystyrene is 53% and only 8% in tensile strength. Again, the mechanically interlocked samples lead to a well-defined improvement, offering 130% and 290% variations in Young's modulus and 140% and 240% increase in tensile strength for MINT(o)−**1** and MINT(o)−**2**, respectively. Just like with the other types of nanotubes, the supramolecular fillers offered no improvements in the mechanical properties over pure polystyrene.

No significant changes were observed in the strain-to-break among samples with the same kind of nanotubes (Figure 4c).

Complex effects could be responsible for the improvement observed in the mechanical properties of the composites, including nanoscale friction at the polymer−nanocarbon interface.[58,59] In order to gain atomic understanding of our system, molecular dynamics (MD) simulations were performed using the AMBER force field,[60] which accounts for dispersion interactions. To mimic our experimental conditions as much as possible, MD calculations were carried out using a (6,5)-SWNT of 400 atoms to ensure the same SWNT/macrocycle ratio measured experimentally. The polystyrene fiber consisted of 36 residues, which were introduced in a fully extended conformation to emulate the electrospinning conditions. Initial configuration of the composites and computational details are described in the Supporting Information. Figure 5 shows the equilibrated structures of polystyrene and its composites with SWNTs, SWNT·**1**, SWNT·**2**, MINT−**1** and MINT−**2**. Due to the flexible backbone, after 0.4 ns a highly twisted, globular structure is adopted to maximize intramolecular interactions (Figure 5a). A

DOI: 10.1021/acsnano.6b04028
ACS Nano 2016, 10, 8012−8018

similar picture dominates the first frames of the simulations with the nanotube fillers, until polymer–nanotube intermolecular interactions become relevant. Upon stabilization (after approximately 2 ns of simulation time, see the Supporting Information), we observe very clear differences between the various fillers. The pristine nanotubes allow polystyrene to adopt a globular structure, very similar to that found for pure polystyrene (Figure 5b). In the supramolecular controls, the fiber tries to maximize short contacts with both macrocycle and SWNT, which results in a slightly more distorted structure (Figure 5c,d). Finally, in the MINT samples the positioning of the macrocycles around the nanotubes results in less surface available for interaction with the polystyrene fiber, which reacts by adopting a significantly more extended conformation in order to maximize noncovalent interactions with the SWNT (Figures 5e and 5f). As a quantitative metric for these observations, we measured the dihedral angles of the polystyrene backbone for each case for a total of 500 frames in the last nanosecond of our simulation (Figure 5g). An average of around 130° is found for the MINTs, compared to an average of 95° for the supramolecular compounds and approximately 105° for the polymer-SWNT model. The extended conformation of polystyrene according to MD simulations is more pronounced in the case of MINT−**1** when compared to MINT−**2**, while the results for the supramolecular models are fundamentally independent of the structure of the macrocycle, in direct correlation with experimental results. Polymer-chain extension and orientation are established prerequisites to produce strong/stiff polymeric materials, for example, in the form of high-performance fibers.[61,62] The MINT-induced polymer conformation extracted from MD simulations is in line with such arrangement and agrees with the higher degree of reinforcement observed for MINT-containing composites.

CONCLUSIONS

In summary, we have shown that mechanical interlocking is a strategy to optimize the performance of SWNT fillers with regard to their mechanical properties. Very low loading of 0.01% results in improvement of the Young's modulus and tensile strength of the fibers of over 200%. In comparison, fillers with identical chemical composition but lacking the interlocked architectures showed negligible or even detrimental effects. Moreover, by using up to three different kinds of nanotubes, two macrocycles, and the corresponding supramolecular controls, we have demonstrated that the positive effect is general to the MINT samples, as the trends hold in all cases under study. MD simulations show that this effect originates from a superior ability of the MINT fillers to induce extended conformation in the polystyrene fibers, which allows for an optimized transfer of stress between matrix and SWNTs.

EXPERIMENTAL METHODS

(6,5)-Enriched nanotubes were purchased from Sigma-Aldrich (0.7−0.9 nm in diameter, length ≥700 nm, mostly semiconducting, 95% purity), plasma-purified SWNTs (pp-SWNTs) were purchased from Cheap Tubes, Inc. (0.8−1.6 nm in diameter, length 3−30 μm, mostly metallic, 99% purity), and COOH-functionalized SWNTs (o-SWNTs) were purchased from Cheap Tubes, Inc. (0.8−1.6 nm in diameter, length 0.5−2.0 μm, mostly metallic, 99% purity). Electrospinning was carried out using a commercially available Spraybase electrospinning system. TGA was performed using a TA Instruments TGAQ500 with a ramp of 10 °C/min under air from 100 to 1000 °C. SEM micrographs were obtained in a Zeiss EVO HD15 operating at 5 kV. UV−vis spectra were obtained in a Varian Cary 50 UV−vis. Mechanical properties were determined using a dynamic mechanical analyzer (DMA Q800, TA Instruments). Each fiber sample (n = 3 specimens) was cut in 1 cm × 4 cm rectangular shapes with thicknesses between 0.15 and 0.18 mm. Stress−strain curves were recorded at a rate of 1 N min^{-1} (up to 18 N).

Linear receptors and MINTs were synthesized as described in refs 42−45. The nanotubes (10 mg) were suspended in 10 mL of tetrachloroethane through sonication (10 min) and mixed with linear precursors **1** and **2** (0.01 mmol) and Grubbs' second-generation catalyst at room temperature for 72 h. After this time, the suspension was filtered through a PTFE membrane of 0.2 μm pore size and the solid washed profusely with dichloromethane (DCM). The solid was resuspended in 10 mL of DCM through sonication for 10 min and filtered through a PTFE membrane of 0.2 μm pore size again. This washing procedure was repeated three times.

Composites were prepared by direct suspension of MINTs or pristine nanotubes in dimethylformamide by sonication at 20 °C for 12 h, and the suspensions were centrifuged at 13150g for 15 min to obtain stable suspensions following the addition of polystyrene (M_w average 350000) 30% (w/w) and stirring for 12 h. In the case of supramolecular samples, pristine nanotubes were suspended under the same conditions, preformed macrocycles were added before polystyrene, and the mixture was stirred for 12 h. Concentrations of SWNTs, MINTs, and supramolecular models were matched using UV−vis spectra at 450 nm of the suspension obtained. The prepared solutions were added to a syringe and pumped at 1 mL h^{-1} with a voltage of 14 kV and constant temperature and humidity. All samples were electrospun over a 10 cm diameter round collector to obtain randomly aligned fibers.

ASSOCIATED CONTENT

Supporting Information

The Supporting Information is available free of charge on the ACS Publications website at DOI: 10.1021/acsnano.6b04028.

Characterization not shown in the main text and computational details (PDF)

AUTHOR INFORMATION

Corresponding Authors

*E-mail: dario.pisignano@unisalento.it.

*E-mail: emilio.perez@imdea.org.

Notes

The authors declare no competing financial interest.

ACKNOWLEDGMENTS

The research leading to these results has received funding from the European Research Council under the European Union's Seventh Framework Programme (FP/2007-2013)/ERC Grant Agreements No. 306357 (ERC Starting Grant "NANO-JETS"), No. 307609 (ERC Starting Grant "MINT"), MINECO (CTQ2014-60541-P, MAT2015-62584-ERC and RyC-2014-15115, Spain), and the MAD2D project (S2013/MIT-3007, Comunidad de Madrid). The computational work was supported by the Campus of International Excellence (CEI) UAM+CSIC. Additionally, we express our gratitude to the Supercomputing and Bioinnovation Center (SCBI) of the University of Málaga (Spain) for their support and resources.

DEDICATION

Dedicated to Prof. Nazario Martín, on the occasion of his 60th birthday.

REFERENCES

(1) Ajayan, P. M.; Stephan, O.; Colliex, C.; Trauth, D. Aligned Carbon Nanotube Arrays Formed by Cutting a Polymer Resin−Nanotube Composite. *Science* **1994**, *265*, 1212−1214.

DOI: 10.1021/acsnano.6b04028
ACS Nano 2016, 10, 8012−8018

(2) Thostenson, E. T.; Ren, Z.; Chou, T. W. Advances in the Science and Technology of Carbon Nanotubes and Their Composites: a Review. *Compos. Sci. Technol.* **2001**, *61*, 1899−1912.
(3) Breuer, O.; Sundararaj, U. Big Returns From Small Fibers: A Review of Polymer/Carbon Nanotube Composites. *Polym. Compos.* **2004**, *25*, 630−645.
(4) Harris, P. J. F. Carbon Nanotube Composites. *Int. Mater. Rev.* **2004**, *49*, 31−43.
(5) Coleman, J. N.; Khan, U.; Blau, W. J.; Gun'ko, Y. K. Small but Strong: A Review of the Mechanical Properties of Carbon Nanotube−Polymer Composites. *Carbon* **2006**, *44*, 1624−1652.
(6) Li, C.; Thostenson, E. T.; Chou, T.-W. Sensors and Actuators Based on Carbon Nanotubes and Their Composites: A Review. *Compos. Sci. Technol.* **2008**, *68*, 1227−1249.
(7) Arash, B.; Wang, Q.; Varadan, V. K. Mechanical Properties of Carbon Nanotube/Polymer Composites. *Sci. Rep.* **2014**, *4*, 6479.
(8) Liu, Y.; Kumar, S. Polymer/Carbon Nanotube Nano Composite Fibers−A Review. *ACS Appl. Mater. Interfaces* **2014**, *6*, 6069−6087.
(9) Vilatela, J. J. Nanocarbon-Based Composites. In *Nanocarbon−Inorganic Hybrids: Next Generation Composites for Sustainable Energy Applications*, Dominik, E., Schlögl, R., Eds.; De Gruyter-GmbH: Berlin, 2014; pp 227−254.
(10) Kong, W.; Sun, L.; Wu, Y.; Jiang, K.; Li, Q.; Wang, J.; Fan, S. Binder-Free Polymer Encapsulated Sulfur−Carbon Nanotube Composite Cathodes for High Performance Lithium Batteries. *Carbon* **2016**, *96*, 1053−1059.
(11) Liu, G.; Ling, Q.-D.; Teo, E. Y. H.; Zhu, C.-X.; Chan, D. S.-H.; Neoh, K.-G.; Kang, E.-T. Electrical Conductance Tuning and Bistable Switching in Poly(N-vinylcarbazole)−Carbon Nanotube Composite Films. *ACS Nano* **2009**, *3*, 1929−1937.
(12) Li, X.; Gittleson, F.; Carmo, M.; Sekol, R. C.; Taylor, A. D. Scalable Fabrication of Multifunctional Freestanding Carbon Nanotube/Polymer Composite Thin Films for Energy Conversion. *ACS Nano* **2012**, *6*, 1347−1356.
(13) Habisreutinger, S. N.; Leijtens, T.; Eperon, G. E.; Stranks, S. D.; Nicholas, R. J.; Snaith, H. J. Carbon Nanotube/Polymer Composites as a Highly Stable Hole Collection Layer in Perovskite Solar Cells. *Nano Lett.* **2014**, *14*, 5561−5568.
(14) Zhu, J.; Cao, W.; Yue, M.; Hou, Y.; Han, J.; Yang, M. Strong and Stiff Aramid Nanofiber/Carbon Nanotube Nanocomposites. *ACS Nano* **2015**, *9*, 2489−2501.
(15) Wang, Y.; Li, M.; Gu, Y.; Zhang, X.; Wang, S.; Li, Q.; Zhang, Z. Tuning Carbon Nanotube Assembly for Flexible, Strong and Conductive Films. *Nanoscale* **2015**, *7*, 3060−3066.
(16) Fadel, T. R.; Sharp, F. A.; Vudattu, N.; Ragheb, R.; Garyu, J.; Kim, D.; Hong, E.; Li, N.; Haller, G. L.; Pfefferle, L. D.; Justesen, S.; Harold, K. C.; Fahmy, T. M. A Carbon Nanotube−Polymer Composite for T-Cell Therapy. *Nat. Nanotechnol.* **2014**, *9*, 639−647.
(17) Gao, J.; Itkis, M. E.; Yu, A.; Bekyarova, E.; Zhao, B.; Haddon, R. C. Continuous Spinning of a Single-Walled Carbon Nanotube−Nylon Composite Fiber. *J. Am. Chem. Soc.* **2005**, *127*, 3847−3854.
(18) Sen, R.; Zhao, B.; Perea, D.; Itkis, M. E.; Hu, H.; Love, J.; Bekyarova, E.; Haddon, R. C. Preparation of Single-Walled Carbon Nanotube Reinforced Polystyrene and Polyurethane Nanofibers and Membranes by Electrospinning. *Nano Lett.* **2004**, *4*, 459−464.
(19) Coleman, J. N.; Khan, U.; Gun'ko, Y. K. Mechanical Reinforcement of Polymers Using Carbon Nanotubes. *Adv. Mater.* **2006**, *18*, 689−706.
(20) Sun, X.; Sun, H.; Li, H.; Peng, H. Developing Polymer Composite Materials: Carbon Nanotubes or Graphene? *Adv. Mater.* **2013**, *25*, 5153−5176.
(21) Stoddart, J. F. The Chemistry of the Mechanical Bond. *Chem. Soc. Rev.* **2009**, *38*, 1802−1820.
(22) Neal, E. A.; Goldup, S. M. Chemical Consequences of Mechanical Bonding in Catenanes and Rotaxanes: Isomerism, Modification, Catalysis and Molecular Machines for Synthesis. *Chem. Commun.* **2014**, *50*, 5128−5142.
(23) Berná, J.; Bottari, G.; Leigh, D. A.; Pérez, E. M. Amide-Based Molecular Shuttles. *Pure Appl. Chem.* **2007**, *79*, 39−54.
(24) Kay, E. R.; Leigh, D. A.; Zerbetto, F. Synthetic Molecular Motors and Mechanical Machines. *Angew. Chem., Int. Ed.* **2007**, *46*, 72−191.
(25) Credi, A.; Venturi, M.; Balzani, V. Light on Molecular Machines. *ChemPhysChem* **2010**, *11*, 3398−3403.
(26) Sauvage, J.-P.; Collin, J.-P.; Durot, S.; Frey, J.; Heitz, V.; Sour, A.; Tock, C. From Chemical Topology to Molecular Machines. *C. R. Chim.* **2010**, *13*, 315−328.
(27) Bruns, C. J.; Stoddart, J. F. Rotaxane-Based Molecular Muscles. *Acc. Chem. Res.* **2014**, *47*, 2186−2199.
(28) Niess, F.; Duplan, V.; Sauvage, J.-P. Molecular Muscles: From Species in Solution to Materials and Devices. *Chem. Lett.* **2014**, *43*, 964−974.
(29) Kay, E. R.; Leigh, D. A. Rise of the Molecular Machines. *Angew. Chem., Int. Ed.* **2015**, *54*, 10080−10088.
(30) Erbas-Cakmak, S.; Leigh, D. A.; McTernan, C. T.; Nussbaumer, A. L. Artificial Molecular Machines. *Chem. Rev.* **2015**, *115*, 10081−10206.
(31) Fang, L.; Olson, M. A.; Benítez, D.; Tkatchouk, E.; Goddard, W. A., III; Stoddart, J. F. Mechanically Bonded Macromolecules. *Chem. Soc. Rev.* **2010**, *39*, 17−29.
(32) Dong, R.; Zhou, Y.; Huang, X.; Zhu, X.; Lu, Y.; Shen, J. Functional Supramolecular Polymers for Biomedical Applications. *Adv. Mater.* **2015**, *27*, 498−526.
(33) Gibson, H. W.; Bheda, M. C.; Engen, P. T. Polycatenanes and Related Materials. *Prog. Polym. Sci.* **1994**, *19*, 843−945.
(34) Takata, T.; Kihara, N.; Furusho, Y. *Polyrotaxanes and Polycatenanes: Recent Advances in Syntheses and Applications of Polymers Comprising of Interlocked Structures*; Springer: Berlin, 2004; pp 1−75.
(35) Huang, F.; Gibson, H. W. Polypseudorotaxanes and Polyrotaxanes. *Prog. Polym. Sci.* **2005**, *30*, 982−1018.
(36) Coelho, J. P.; González-Rubio, G.; Delices, A.; Barcina, J. O.; Salgado, C.; Ávila, D.; Peña-Rodríguez, O.; Tardajos, G.; Guerrero-Martínez, A. Polyrotaxane-Mediated Self-Assembly of Gold Nanospheres into Fully Reversible Supercrystals. *Angew. Chem., Int. Ed.* **2014**, *53*, 12751−12755.
(37) Park, I.-H.; Medishetty, R.; Kim, J.-Y.; Lee, S. S.; Vittal, J. J. Distortional Supramolecular Isomers of Polyrotaxane Coordination Polymers: Photoreactivity and Sensing of Nitro Compounds. *Angew. Chem., Int. Ed.* **2014**, *53*, 5591−5595.
(38) Montarnal, D.; Delbosc, N.; Chamignon, C.; Virolleaud, M.-A.; Luo, Y.; Hawker, C. J.; Drockenmuller, E.; Bernard, J. Highly Ordered Nanoporous Films from Supramolecular Diblock Copolymers with Hydrogen-Bonding Junctions. *Angew. Chem., Int. Ed.* **2015**, *54*, 11117−11121.
(39) Goujon, A.; Du, G.; Moulin, E.; Fuks, G.; Maaloum, M.; Buhler, E.; Giuseppone, N. Hierarchical Self-Assembly of Supramolecular Muscle-Like Fibers. *Angew. Chem., Int. Ed.* **2016**, *55*, 703−707.
(40) Tao, X.; Liu, J.; Koley, G.; Li, X. B/SiO_x Nanonecklace Reinforced Nanocomposites by Unique Mechanical Interlocking Mechanism. *Adv. Mater.* **2008**, *20*, 4091−4096.
(41) Ni, H.; Li, X. Self-Assembled Composite Nano-/Micronecklaces with SiO_2 Beads in Boron Strings. *Appl. Phys. Lett.* **2006**, *89*, 053108.
(42) de Juan, A.; Pouillon, Y.; Ruiz-González, L.; Torres-Pardo, A.; Casado, S.; Martín, N.; Rubio, Á.; Pérez, E. M. Mechanically Interlocked Single-Wall Carbon Nanotubes. *Angew. Chem., Int. Ed.* **2014**, *53*, 5394−5400.
(43) de Juan, A.; Mar Bernal, M.; Pérez, E. M. Optimization and Insights into the Mechanism of Formation of Mechanically Interlocked Derivatives of Single-Walled Carbon Nanotubes. *ChemPlusChem* **2015**, *80*, 1153−1157.
(44) López-Moreno, A.; Pérez, E. M. Pyrene-Based Mechanically Interlocked SWNTs. *Chem. Commun.* **2015**, *51*, 5421−5424.
(45) Martínez-Periñan, E.; de Juan, A.; Pouillon, Y.; Schierl, C.; Strauss, V.; Martín, N.; Rubio, A.; Guldi, D. M.; Lorenzo, E.; Pérez, E. M. The Mechanical Bond on Carbon Nanotubes: Diameter-Selective Functionalization and Effects on Physical Properties. *Nanoscale* **2016**, *8*, 9254−9264.
(46) de Juan, A.; López-Moreno, A.; Calbo, J.; Ortí, E.; Pérez, E. M. Determination of Association Constants Towards Carbon Nanotubes. *Chem. Sci.* **2015**, *6*, 7008−7014.

DOI: 10.1021/acsnano.6b04028
ACS Nano 2016, 10, 8012−8018

(47) Wurl, A.; Goossen, S.; Canevet, D.; Sallé, M.; Pérez, E. M.; Martín, N.; Klinke, C. Supramolecular Interaction of Single-Walled Carbon Nanotubes with a Functional TTF-Based Mediator Probed by Field-Effect Transistor Devices. *J. Phys. Chem. C* **2012**, *116*, 20062−20066.
(48) Pérez, E. M.; Illescas, B. M.; Herranz, M. Á.; Martín, N. Supramolecular Chemistry of [Small Pi]-Extended Analogues of TTF and Carbon Nanostructures. *New J. Chem.* **2009**, *33*, 228−234.
(49) Romero-Nieto, C.; García, R.; Herranz, M. Á.; Ehli, C.; Ruppert, M.; Hirsch, A.; Guldi, D. M.; Martín, N. Tetrathiafulvalene-Based Nanotweezers—Noncovalent Binding of Carbon Nanotubes in Aqueous Media with Charge Transfer Implications. *J. Am. Chem. Soc.* **2012**, *134*, 9183−9192.
(50) Amabilino, D. B.; Pérez-García, L. Topology in Molecules Inspired, Seen and Represented. *Chem. Soc. Rev.* **2009**, *38*, 1562−1571.
(51) Griffiths, K. E.; Stoddart, J. F. Template-Directed Synthesis of Donor/Acceptor [2]Catenanes and [2]Rotaxanes. *Pure Appl. Chem.* **2008**, *80*, 485−506.
(52) de Juan, A.; Pérez, E. M. Getting Tubed: Mechanical Bond in Endohedral Derivatives of Carbon Nanotubes? *Nanoscale* **2013**, *5*, 7141−7148.
(53) Ko, F.; Gogotsi, Y.; Ali, A.; Naguib, N.; Ye, H.; Yang, G. L.; Li, C.; Willis, P. Electrospinning of Continuous Carbon Nanotube-Filled Nanofiber Yarns. *Adv. Mater.* **2003**, *15*, 1161−1165.
(54) Hou, H.; Ge, J. J.; Zeng, J.; Li, Q.; Reneker, D. H.; Greiner, A.; Cheng, S. Z. D. Electrospun Polyacrylonitrile Nanofibers Containing a High Concentration of Well-Aligned Multiwall Carbon Nanotubes. *Chem. Mater.* **2005**, *17*, 967−973.
(55) Dror, Y.; Salalha, W.; Khalfin, R. L.; Cohen, Y.; Yarin, A. L.; Zussman, E. Carbon Nanotubes Embedded in Oriented Polymer Nanofibers by Electrospinning. *Langmuir* **2003**, *19*, 7012−7020.
(56) Fasano, V.; Baroncini, M.; Moffa, M.; Iandolo, D.; Camposeo, A.; Credi, A.; Pisignano, D. Organic Nanofibers Embedding Stimuli-Responsive Threaded Molecular Components. *J. Am. Chem. Soc.* **2014**, *136*, 14245−14254.
(57) Mazinani, S.; Ajji, A.; Dubois, C. Morphology, Structure and Properties of Conductive Polystyrene/CNT Nanocomposite Electrospun Mat. *Polymer* **2009**, *50*, 3329−3342.
(58) Vilhena, J. G.; Pimentel, C.; Pedraz, P.; Luo, F.; Serena, P. A.; Pina, C. M.; Gnecco, E.; Pérez, R. Atomic-Scale Sliding Friction on Graphene in Water. *ACS Nano* **2016**, *10*, 4288−4293.
(59) Karuppiah, K. S. K.; Sundararajan, S.; Xu, Z.-H.; Li, X. The Effect of Protein Adsorption on the Friction Behavior of Ultra-High Molecular Weight Polyethylene. *Tribol. Lett.* **2006**, *22*, 181−188.
(60) Hornak, V.; Abel, R.; Okur, A.; Strockbine, B.; Roitberg, A.; Simmerling, C. Comparison of Multiple Amber Force Fields and Development of Improved Protein Backbone Parameters. *Proteins: Struct., Funct., Genet.* **2006**, *65*, 712−725.
(61) Staudinger, H. In *Die Hochmolekularen Organischen Verbindungen - Kautschuk und Cellulose*; Springer: Berlin, 1932.
(62) Carothers, W. H.; Hill, J. W. Studies of Polymerization and Ring Formation. XV. Artificial Fibers from Synthetic Linear Condensation Superpolymers. *J. Am. Chem. Soc.* **1932**, *54*, 1579−1587.

DOI: 10.1021/acsnano.6b04028
ACS Nano 2016, 10, 8012−8018